Switching Catalyst Selectivity via the Introduction of a Pendant Nitrophenyl Group

Eric M. Johnson, Jeffrey J. Liu, Adam D. Samuel, Ralf Haiges, Smaranda C. Marinescu* Department of Chemistry, University of Southern California, Los Angeles, California 90089, United States

*email: smarines@usc.edu

ABSTRACT

The conversion of abundant small molecules to value-added products serves as an attractive method to store renewable energy in chemical bonds. A family of macrocyclic cobalt aminopyridine complexes was previously reported to reduce CO₂ to CO with 98% faradaic efficiency through the formation of hydrogen bonding networks, and with the number of secondary amines affecting catalyst performance. One of these aminopyridine macrocycles, (NH)₁(NMe)₃-Bridged Calix[4]pyridine (L⁵), was modified with a nitrophenyl group to form L^{NO2} and metallated with a cobalt(II) precursor to generate CoL^{NO2}, which would allow for probing the positioning and steric effects on catalysis. The addition of a nitrophenyl moiety to the ligand backbone results in a drastic shift in selectivity. Large current increases in the presence of added protons and CoLNO2 are observed under both N2 and CO2. The current increases under N2 are approximately 30 times larger than the ones under CO2, suggesting a change in the selectivity of CoL^{NO2} to favor H₂ production versus CO₂ reduction. H₂ is determined to be the dominant reduction product by gas chromatography, reaching faradaic efficiencies up to 76% under N2 with TFE, and 71% under CO2 with H2O, in addition to small amounts of formate. X-ray photoelectron spectroscopy (XPS) reveal the presence of a cobalt containing heterogeneous deposit on the working electrode surface indicating the addition of the nitrophenyl group reduces the electrochemical stability of the catalyst. These observed catalytic behaviors are demonstrably different relative to the tetra-NH bridged macrocycle, which shows 98% Faradaic efficiency for CO₂-to-CO conversion with TFE, highlighting the importance of pendant hydrogen bond donors and electrochemically robust functional groups for selective CO₂ conversion.

INTRODUCTION

The divestment in fossil fuels in favor of renewable sources is hindered by the limited ability to store this energy for use when it is most needed.^{1,2} To combat these spatio-temporal issues, the storage of energy in the form of chemical bonds is necessary to effectively decrease reliance on fossil fuels.^{1,3–7} Solar energy can be used to drive chemical reactions such as the hydrogen evolution reaction (HER) and carbon dioxide reduction to produce value-added chemicals.^{5,8–14} Of these two processes, CO₂ reduction is more challenging due to its higher energetic barrier, multiple possible reduction products, and competition with hydrogen evolution.^{5,13–17} In order to develop ideal catalytic systems, extensive optimization is carried out with promising catalysts in order to best understand their properties.

Many successful catalysts for the CO₂ reduction reaction (CO₂RR) with high faradaic efficiency (FE > 95%) for a given product have been developed throughout the years, 5,8 but many of these catalysts exhibit switchable selectivity where a change in the electrochemical conditions, ligand design, or metal center drastically shift the selectivity. Iron porphyrins are well known as selective CO₂-to-CO reduction catalysts, ^{18–24} but their activity can be changed upon the addition of Lewis acid species (e.g. Mg²⁺) to 30% formate production.^{25,26} The addition of a weak Brønsted acid, such as 1-propanol, also facilitates formate production, yielding 35% formate and 60% CO.^{27,28} Cobalt porphyrins have been studied as CO₂ reduction catalysts as well, but have shown higher H₂ production than their iron counterparts.^{29,30,39,31–38} Nickel cyclams are conventionally CO₂-to-CO reduction catalysts, 40-47 but their selectivity is dependent on solvent choice. For example, aprotic solvents favor formic acid production (faradaic efficiency of 75%),⁴² aqueous conditions from pH 4 to 5 and wet organic solvents show high selectivity for CO production, 42-44 whereas highly acidic aqueous solutions (pH < 2) lead to H₂ formation in appreciable yields.⁴⁵ Recently a series of cobalt pyridine thiolate complexes have been shown to exhibit switchable CO₂RR selectivity based on modification of the primary sphere.48-50 coordination When donor the phosphine dppe [dppe 1,2-bis-(diphenylphosphino)ethane] is present, near quantitative conversion of CO₂ to CO (FE_{CO} = 92-95%) is observed, 49,51 whereas in the absence of dppe, formate becomes the major product $(FE_{COOH} = 57\% - 64\%, FE_{CO2} = 2.5 - 7\%)$. Other changes in selectivity have been reported for a cobalt N5 macrocyclic complex where upon replacing the cobalt center with iron the

selectivity changes from primarily CO_2 to CO conversion ($FE_{CO} = 82\%$) to CO_2 to formate ($FE_{COOH} = 75-80\%$).⁵²

The installation of pendant groups is typically proposed as a method to enhance catalytic activity, but changes to the ligand scaffold can have deeper impacts than intended. An iron carbonyl cluster has been shown to reduce CO₂ to formate with faradaic efficiencies near unity, even in aqueous conditions.^{53–55} Modification of this catalyst with a pendant group in the form of PPh₂(CH₂)₂OH caused a complete shift in its reactivity from CO₂-to-formate to hydrogen evolution, producing almost no formate.⁵⁶ Further attempts to modify this catalyst resulted in complexes with similar HER selectivity, with both the pK_a of the substituent and the group size affecting product formation.⁵⁷ Similarly, modification of the bipyridine backbone of [Mn(bpy)(CO)₃Br] with a 2,6-dihydroxyphenyl substituent results in a complex that generates formate with faradaic efficiencies of 36-39% in the presence of mild acids, in addition to drastically reduced amounts of CO.58 Modification of a [Re(bpy)(CO)₃Br] catalyst with amine groups at the 6,6'-bipyridine position results in a catalyst that displays a linear trend between the faradaic efficiency for CO (FE_{CO}) and the electrochemical potential, with the greatest selectivity for CO, 83%, occurring at -2.30 V vs Fc^{+/0}.⁵⁹ Varying amounts of H₂ were also observed with this catalyst in comparison to the unmodified [Re(bpy)(CO)₃Br] catalyst, which is selective for CO₂-to-CO conversion, suggesting a change in the electrocatalyic behavior for the catalyst with pendant proton replays.

Our group has recently reported a series of cobalt aminopyridine macrocycles for the selective reduction of CO_2 to $CO_2^{60,61}$ These complexes contain four pyridines, which are bridged by four amines, with each amine being secondary or tertiary. In this system, the number of secondary amines largely influences catalysis. The k_{obs} increases from 20 s⁻¹ to 16,900 s⁻¹ and the selectivity increases from 36% to 98% FE for CO production when comparing the complex with all four tertiary amines (CoL^6) to the one with all four secondary amines (CoL^1) (Figure 1).⁶¹ It was initially hypothesized that these secondary amines were involved in intramolecular proton-transfer events,⁶⁰ however, density functional theory (DFT) calculations revealed that these groups were actually engaging in hydrogen bonding interactions with added proton sources. As shown by previous reports of porphyrin complexes containing pendant proton donor groups, slight changes in the position of the proton donor groups can have a large impact on the

overall performance of the catalyst.⁶² By making use of the secondary amines that can be further functionalized, the aminopyridine macrocycle can be modified to position the pendant groups in a different orientation for direct ligand-substrate interactions.

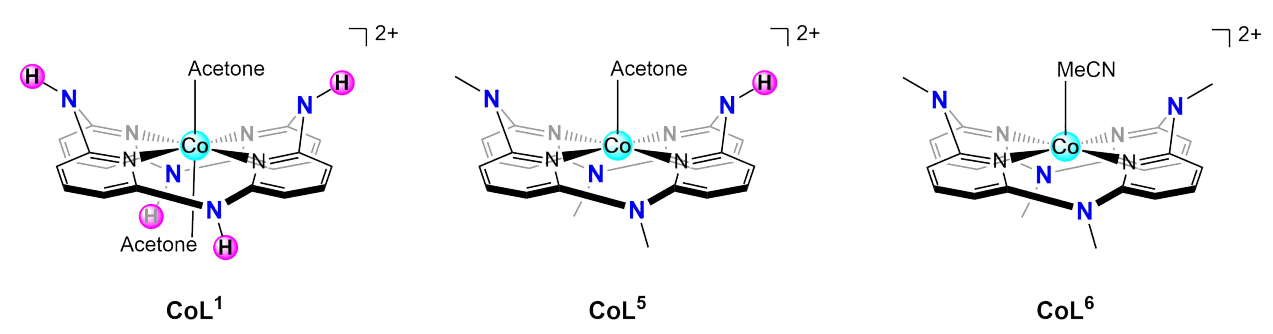


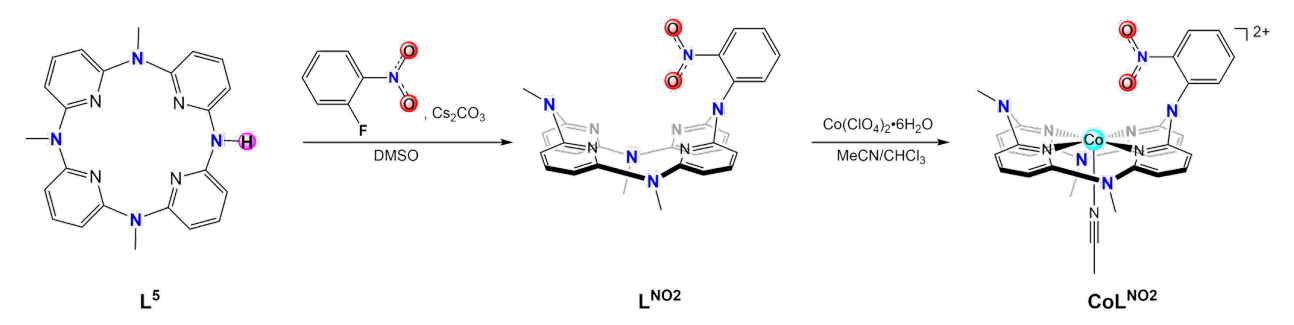
Figure 1. Schematic representations of the unsubstituted cobalt aminopyridine complexes CoL¹ (left), CoL⁵ (middle), CoL⁶ (right).

A modified version of the cobalt aminopyridine cycle was synthesized having a pendant nitrophenyl group, and its effect on the catalyst performance was explored. The complex was characterized, and its electrochemical behavior was investigated to determine its performance relative to the unsubstituted cobalt aminopyridine complexes. Electrochemistry was performed with various proton sources, in different solvents, and under different gaseous atmospheres to understand changes in behavior caused by the introduction of the nitrophenyl group.

RESULTS AND DISCUSSION

Synthesis and Characterization

The macrocycle, (NH)₁(NMe)₃-Bridged Calix[4]pyridine (L⁵), was synthesized according to literature precedent.⁶³ The nitrophenyl modified ligand, L^{NO2}, was synthesized using previously reported methods,⁶⁴ where L⁵, cesium carbonate, and 1-fluoro-2-nitrobenzene were heated in DMSO at 60 °C for 24 hours. After extraction with ethyl acetate, the resulting residue was purified by column chromatography with 2:1 ethyl acetate/hexanes to yield L^{NO2} as a brown solid (Scheme 1).



Scheme 1. Synthesis of L^{NO2} from L^5 and synthesis of CoL^{NO2} from L^{NO2} .

Cobalt(II) perchlorate hexahydrate and L^{NO2} were dissolved in equal amounts of acetonitrile and chloroform, respectively. The two solutions were mixed and stirred for 30 minutes, before removing the solvents to yield CoLNO2 as a brown solid in quantitative yields. The ¹H NMR spectrum of CoL^{NO2} in CD₃CN displays broad peaks (Figure S1), as expected for a paramagnetic species. When using pyridine- d_5 as the NMR solvent, four peaks appear in the ¹H NMR spectrum at δ 31.50, 28.82, 25.36, and 22.37 ppm in a 1:1:1:1 ratio (Figure S2). These peaks are noticeably absent from the ¹H NMR spectrum of the unsubstituted cobalt macrocyle analogue CoL⁵ (Figures 1 and S2), which indicates that the four peaks in the ¹H NMR spectrum of CoL^{NO2} in pyridine- d_5 correspond to the aryl protons of the pendant nitrophenyl moiety. The UV-Vis spectrum of CoL^{NO2} taken in a DMF solution shows two main features: a large peak at 311 nm and a smaller peak at 660 nm, as well as shoulders at 359 nm and 427 nm (Figure S3). These values are consistent with the ones reported previously for this compound when it was formed and characterized through *in-situ* UV-Vis experiments.⁶⁴ FTIR spectra for L^{NO2} (Figure S4) and CoL^{NO2} (Figure S5) display similar features, with the peaks corresponding to the nitro group appearing at 1524 and 1360 cm⁻¹ for both (Figure S6). These results indicate that the electronic environment of the pendant nitrophenyl moiety is identical in the ligand L^{NO2} and the corresponding metal complex, CoL^{NO2}.

X-ray quality crystals of CoL^{NO2} were grown via vapor diffusion of diethyl ether into a chloroform/acetonitrile solution of the complex. Two perchlorate anions and one cobalt aminopyridine complex are present in the asymmetric unit, indicating a dicationic cobalt species. The four pyridine groups of the macrocycle coordinate the cobalt metal center in a square planar geometry, with the bridging amines puckering alternatively up and down (Figure 2). A similar coordination mode was observed for the previously reported aminopyridine complexes.^{60,61,64} A

single acetonitrile solvent molecule is coordinated axially to the cobalt center opposite the face containing the pendant nitrophenyl moiety. A similar singly-solvated X-ray structure was reported for the complexes CoL⁵ and CoL⁶, which contain a coordinated acetone and acetonitrile molecule, respectively, while the cobalt aminopyridine complex containing only secondary amines (four NH moieties) (CoL¹) has two solvent molecules (acetone) coordinated (Figure 1).^{60,61} The pendant nitrophenyl moiety in CoL^{NO2} is positioned over the cobalt metal center, and the Co(1)–O(2) distance is 2.838(4) Å. This value is smaller than the combined Van der Waals radii for oxygen and cobalt (3.52 Å), suggesting that pendant nitrophenyl moiety has a weak interaction with the cobalt center.^{65,66} There is a slight contraction of the Co–N_{Py} and Co–N_(CH3CN) bond lengths in CoL^{NO2} relative to the ones observed in CoL⁵ and CoL⁶ (Table 1).⁶¹ The average Co–N_{Py} bond lengths are 1.925(2) Å for CoL^{NO2}, 1.943(2) Å for CoL⁵, and 1.944(7) Å for CoL⁶, suggesting that the presence of the pendant nitrophenyl moiety leads to a slight increase in the electron density around the cobalt center, and shorter Co–N_{Py} bond lengths.

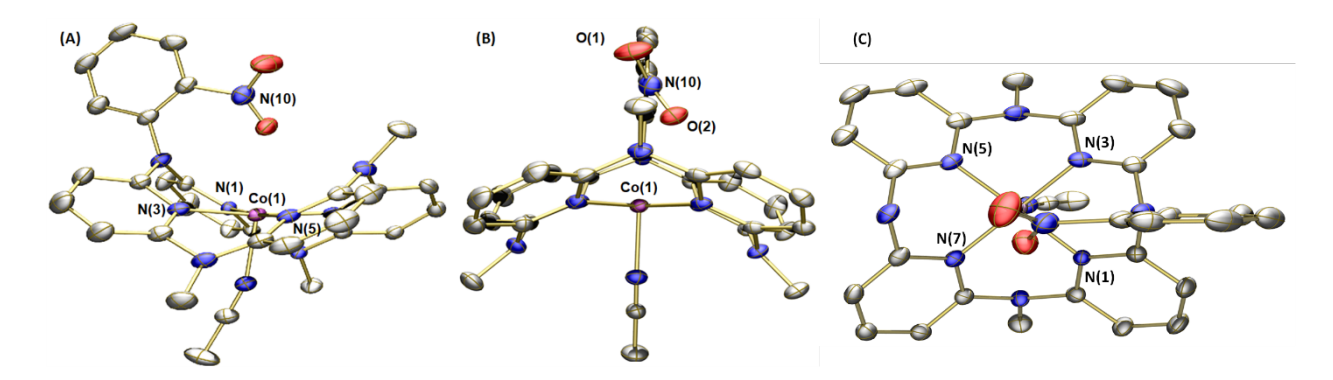


Figure 2. Solid state structure of **CoL**^{NO2} with side (A and B) and top (C) views. Non-coordinating counter ions, unbound solvent species, and hydrogen atoms are omitted for clarity.

Atoms	Atomic Distance, Å (CoL ^{NO2})	Atomic Distance, Å (CoL ⁵)	Atomic Distance, Å (CoL ⁶)
Со-О	2.838(4)		
$Co-X_{(solvent)}$ $(X = N, O)$	2.161(3) Co-N _(CH3CN)	2.223(3) Co-O _(acetone)	2.2046(13) Co-N _(CH3CN)
Co-N _{Py1}	1.929(3)	1.956(4)	1.9498(12)
Co-N _{Py2}	1.928(2)	1.938(4)	1.9383(12)
Co-N _{Py3}	1.925(2)	1.939(4)	1.9419(12)

Co-N _{Py4}	1.919(3)	1.940(4)	1.9492(12)
Reference	this work	61	60

Table 1. Comparison of atomic distances in CoL^{NO2} and the unsubstituted cobalt aminopyridine complexes CoL^5 and CoL^6

Cyclic Voltammetry in Acetonitrile

The ligand L^{NO2} was analyzed electrochemically using cyclic voltammetry (CV) in a 0.1 M tetrabutylammonium hexafluorophosphate (TBAPF₆) acetonitrile solution. All the reduction potentials are referenced versus $Fc^{+/0}$. Under an inert N_2 atmosphere, weak reduction features were observed at -1.65 V and -2.20 V vs $Fc^{+/0}$, along with oxidative features at -1.62 V and -1.18 V (Figure S7). The weak feature observed at approximately -2.7 V is present in a blank solution and is not attributed to any reduction events involving L^{NO2} (Figure S44). When the gaseous atmosphere is changed from N_2 to CO_2 , a small increase in the current density (<0.5 mA/cm²) is observed for the free ligand L^{NO2} at potentials more negative than the second reduction event. Addition of 0.09 M 2,2,2-trifluoroethanol (TFE) as the proton source, leads to a current increase, with subsequent additions of TFE causing only minimal increases until saturation at 0.65 M TFE (Figure S8). These results indicate that the free ligand L^{NO2} displays small current increases in the presence of CO_2 , or CO_2 and protons.

CVs of the metal complex CoL^{NO2} under a nitrogen atmosphere showed three reduction events at -0.95 V, -1.75 V, and -2.43 V (Figures 3A and 4). The CV of a 0.1 M TBAPF6 acetonitrile solution is illustrated in Figure S44. A Zn analog, ZnL^{NO2}, was synthesized for comparison and its electrochemistry was explored (Figure 4). Comparison of the CVs under N₂ for L^{NO2}, CoL^{NO2}, and ZnL^{NO2} (Figure 4), reveals different electrochemical behavior for each species. The ligand L^{NO2} displays two weak redox events, as stated above. However, the cobalt species CoL^{NO2} displays three features with the peak at -1.75 V appearing to be larger in magnitude than the other two features at -0.95 V and -2.43 V, suggesting that the feature at -1.75 V corresponds to a multi-electron reduction. The Zn analogue, ZnL^{NO2}, shows no significant features compared to L^{NO2} and CoL^{NO2}. The reductive features at -1.75 V and -2.43 V for CoL^{NO2} are reminiscent of the ones previously reported for the CoL¹⁻⁶ series, which all exhibit reversible Co^{11/1} couples and irreversible Co^{1/0} reductions.⁶¹ The weak return oxidative feature on the anodic scan near -1.5 V (Figures 3A and S9) is consistent with a quasi-reversible

Co^{II/I} couple, while the feature at -2.43 V can be assigned to the Co^{II/O} reduction (Table 2). The remaining reduction at -0.95 V and a portion of the current at -1.75 V are assigned to positively shifted irreversible ligand-based reductions (observed at -1.65 V and -2.20 V in L^{NO2}) where the second ligand-based reduction overlaps with the Co^{II/I} reduction resulting in the large current response at -1.75 V (Table 2). A plot of log(scan rate) vs log(current) for the couple at -1.75 V vs Fc^{+/O} yields a linear relationship with a slope of approximately 0.5, which is indicative of a freely-diffusing species in solution according to the Randles-Sevcik equation (Figures S9). Thus, the three features in CoL^{NO2} CV are assigned to a combination of ligand-based (-0.95 V and -1.75 V) and cobalt-based (-1.75 V and -2.43 V) reductions.

Table 2. Electrochemical and electrocatalytic properties of CoL¹, CoL⁵, CoL⁶, and CoL^{NO2}.
^aPotentials measured vs. Fc^{+/0} under 1 atmosphere of N₂.
^bExperiments performed in DMF with 0.1 M TBAPF₆; controlled potential electrolysis performed at -2.75 V vs. Fc^{+/0} for 2 hours with 1.2 M TFE under 1 atmosphere CO₂.
^cExperiments performed in MeCN with 0.1 M TBAPF₆; controlled potential electrolysis performed at -2.70 V vs. Fc^{+/0} for 2 hours with 1.0 M TFE under 1 atmosphere CO₂.
^dNo H₂ detected.

	$E_{1/2}(Co^{II/I})(V)^a$	$E(Co^{1/0})(V)^a$	$E(L^0/L^-)(V)^a$	$E(L^{-}/L^{2-})(V)^a$	FE _{CO} (%)	FE _{H2} (%)	Ref
CoL ^{1 b}	-1.65	-2.46	N/A	N/A	98	d	61
CoL ^{5 b}	-1.44	-2.87	N/A	N/A	90	d	61
CoL ^{6 b}	-1.41	-2.58	N/A	N/A	36	d	61
L ^{NO2 c}	N/A	N/A	-1.65	-2.20	-	-	This Work
CoL ^{NO2 c}	-1.75	-2.43	-0.95	-1.75	4	17	This Work

Addition of 0.87 M TFE to a 0.5 mM CoL^{NO2} acetonitrile solution under N_2 results in a large current increase, reaching a current density of 82 mA/cm² at -2.90 V vs Fc^{+/0} (Figures 3B and S10). The return oxidation scan crosses over the reduction trace, indicating either decomposition of the molecular species, or the fact that the reduced product accumulates at the eletrode interfaces, and diffuses away slower in comparison with the backward oxidation reaction.

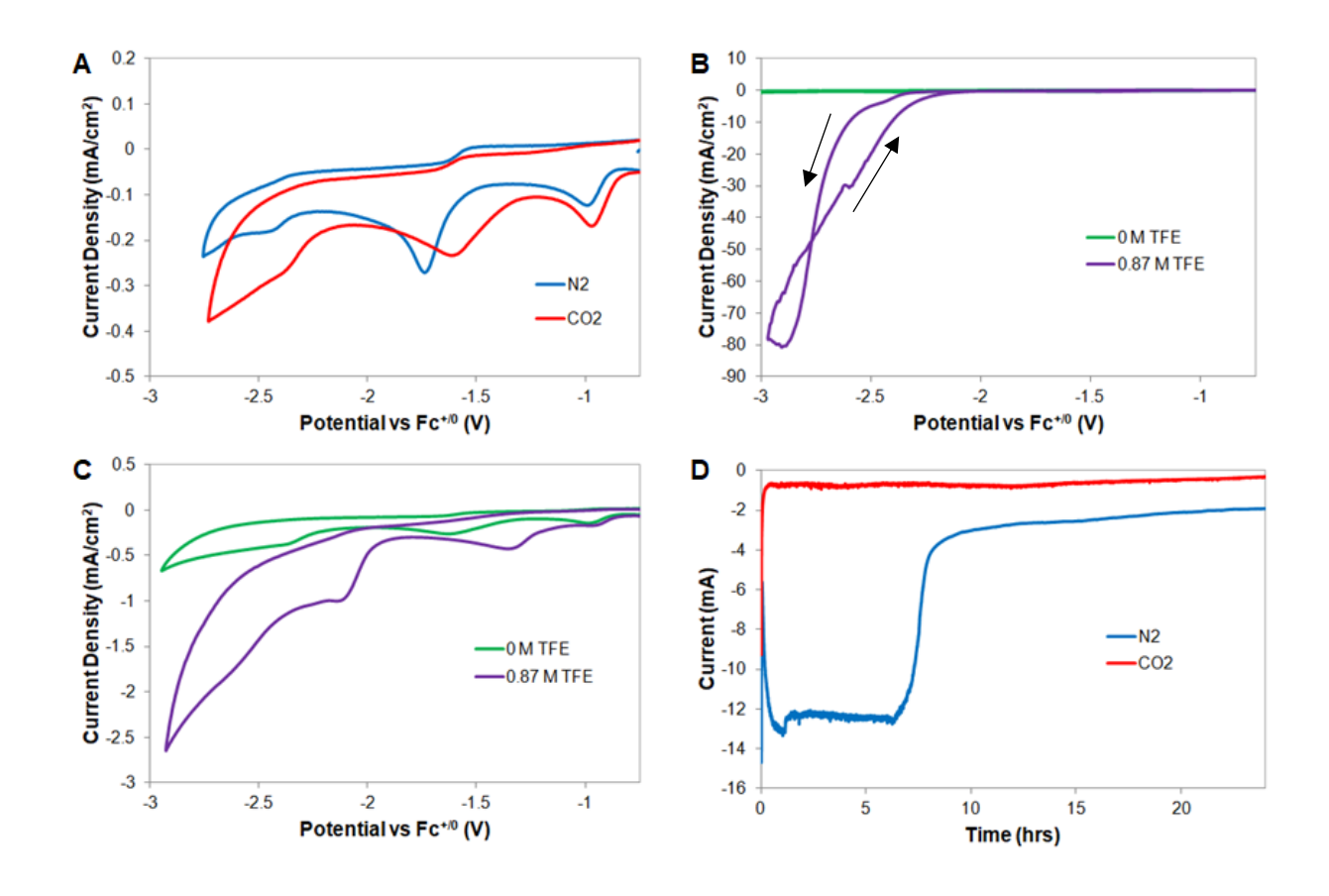


Figure 3. (A) CVs of 0.5 mM **CoL**^{NO2} under N₂ (blue) and CO₂ (red) atmospheres in 0.1 M TBAPF₆ MeCN solution. (B) CVs of 0.5 mM **CoL**^{NO2} under an N₂ atmosphere with 0 M TFE (green) and 0.87 M TFE (purple) added in 0.1 M TBAPF₆ MeCN solution. (C) CVs of 0.5 mM **CoL**^{NO2} under a CO₂ atmosphere with 0 M TFE (green) and 0.87 M TFE (purple) added in 0.1 M TBAPF₆ MeCN solution. (D) Controlled potential electrolysis of 0.5 mM **CoL**^{NO2} under N₂ (blue) and CO₂ (red) with 0.87 M TFE in 0.1 M TBAPF₆ MeCN solution.

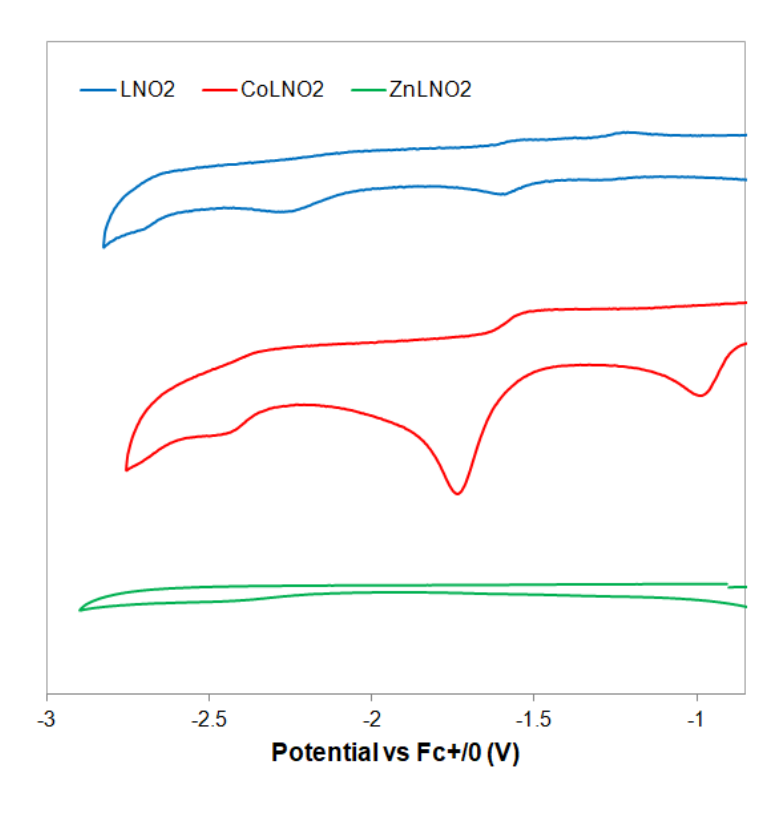


Figure 4. CVs overlay of L^{NO2} (blue), CoL^{NO2} (red), and ZnL^{NO2} (green) in 0.1 M TBAPF₆ acetonitrile solution under N_2 . Scan rate = 100 mV/s.

Upon changing the atmosphere from N₂ to CO₂, CoL^{NO2} displays only a minor current increase and slight anodic shifts of the –1.75 V and –2.43 V reduction features (Figure 3A), in comparison to the behavior observed for the free ligand L^{NO2} (Figure S7). This is not consistent with the behavior observed for the unsubstituted aminopryridine complexes, where a noticeable increase was reported when changing the atmosphere from N₂ to CO₂.^{60,61} However, current increases are observed upon addition of TFE to CoL^{NO2} under CO₂ (Figures 3C and S11). It is important to emphasize, however, that the currents reached under CO₂ are roughly 30-fold less than the ones under an N₂ atmosphere. Under both CO₂ and N₂, the addition of TFE causes an anodic shift in the reduction feature at –1.75 V (Figures 5, S8, and S11), which has been linked to the binding of a substrate to the reduced metal complex.^{67–70} In this particular case, the TFE dependent positive shift of the Co^{II/I} reduction wave is consistent with the formation of an Co^I-acid adduct. Such behavior has not been observed in the CoL^{I-6} series, suggesting the introduction of the nitrophenyl moiety results in a change in the electrochemical behavior.

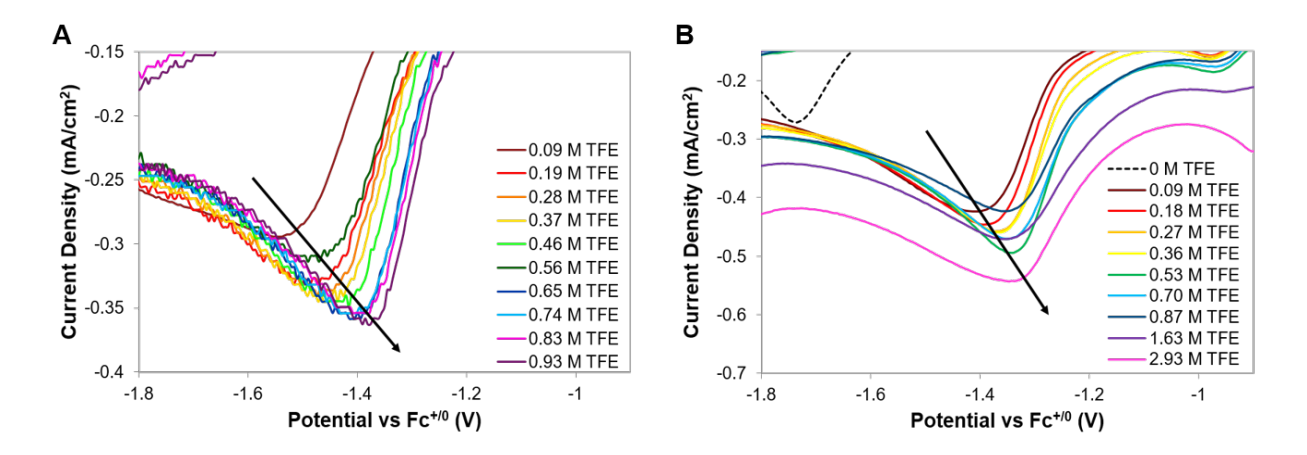


Figure 5. CVs of 0.5 mM CoL^{NO2} in 0.1 M TBAPF₆ MeCN solution under a N₂ (A) and CO₂ (B) atmospheres with increasing amounts of TFE focused on the reduction event at -1.75 V vs $Fc^{+/0}$, which shifts anodically. Full scans of the above voltammograms can be found in the supporting information (Figures S8 and S11, respectively).

Different acid sources were also tested for the activity of CoL^{NO2} under CO_2 or N_2 . Titrating with water results in a similar behavior to the one observed for the TFE titrations, with N_2 scans reaching 15.2 mA/cm² at -2.68 V, and CO_2 scans reaching 3.76 mA/cm² at -2.55 V upon the addition of 13.8 M H_2O (Figures S12 and S13, respectively). Phenol also displays significant current increases under N_2 with a current of 70 mA/cm² at -2.70 V with 1.67 M (Figure S14). Under CO_2 , a current of 31 mA/cm² is reached at -2.65 V under the same acid concentration (Figures S15 and S16). Overall, a catalytic current increase was observed under all acids tested with a greater increase occurring under N_2 rather than CO_2 atmosphere. At approximately 1 M of added acid, a current enhancement trend of TFE > Phenol > H_2O (Figures S10, S12 and S14) is measured under N_2 atmosphere, while Phenol > TFE > H_2O (Figures S11, S13, and S15) is measured under CO_2 atmosphere.

Controlled Potential Electrolysis

CPE Experiments with 2,2,2-trifluoroethanol Under a N₂ Atmosphere

Controlled potential electrolysis (CPE) studies were performed in acetonitrile at -2.70 V vs Fc^{+/0}. The electrolysis potential was chosen because of the large measured i_{cat} at that potential, and to allow comparisons with the previous studies conducted on the CoL^{1-6} series.⁶¹ Acetonitrile was chosen as the solvent due to the deleterious solvent decarbonylation being observed in DMF (Figure S45 and Table S13). Under an N₂ atmosphere with 0.87 M TFE as the

proton source (Figure 3D) H₂ was produced as the sole reduction product, reaching a faradaic efficiency (FE) of 76% after 2 hours (Table S1). The current was relatively stable during the first 8 hours of the CPE experiment, followed by a rapid decrease in current recorded between the 8-and 10-hour mark. The gas chromatography (GC) analysis performed throughout the 24h CPE experiment reveals a continuous decrease in the faradaic efficiency for H₂ from 76% after 2h, to 45% at the end of the 24h CPE study, with no detected carbon-based reduction products. The production of H₂ is unexpected as CoL⁶ generated no hydrogen gas. These results indicate that the selectivity of the catalyst has been altered by the introduction of the pendant nitrophenyl moiety. The CPE results coupled with the CV studies indicate that under a N₂ atmosphere, CoL^{NO2} catalyzes the hydrogen evolution reaction, and this behavior is similar to the one displayed by other polypyridyl systems which generate H₂ at large overpotentials.⁷¹

X-ray photoelectron spectroscopic (XPS) analysis of the post-electrolysis working electrode reveals the presence of a cobalt species following electrode rinsing, indicating the presence of heterogeneously deposited species (Figure S41). UV-vis analysis of the post-electrolysis solution indicates a general bleaching of the absorption features ascribed to the molecular species (Figure S35), while FTIR of the same post-electrolysis solution shows primarily vibrations resulting from the electrolyte (Figure S38).

CPE Experiments with 2,2,2-trifluoroethanol Under a CO₂ Atmosphere

When the atmosphere is switched from N_2 to CO_2 , the amount of charge passed in the 24h CPE experiment under CO_2 (7.7 C) was much lower than that under N_2 (152.6 C) despite a non-negligible amount of current being passed in the CV under CO_2 (Figures 3C & 3D). After a 2h CPE under CO_2 , 6.7 µmol of H_2 (FE = 17%) and 1.8 µmol of CO (FE = 4%) were detected (Table S2), which was much lower than the amount of H_2 (599.8 µmol; FE = 76%) obtained under a nitrogen atmosphere. Over the 24h CPE study under CO_2 , the FE for H_2 increased from 17% after 2 h to 58% after 24 h, while the FE for CO remained almost constant between 4% and 2%. At the end of the 24-hour CPE, one major product, H_2 (FE = 58%), was detected in addition to two minor products, CO (FE = 2%) and formate (FE = <1%) (Table S2). The presence of formate is typically indicative of a metal hydride intermediate, with some exceptions, 72 as CO_2 insertion into a metal hydride is the primary method of formate production. CPE studies of the unsubstituted cobalt aminopyridine complexes produced exclusively CO under identical

conditions.^{60,61} The addition of the pendant nitrophenyl group has caused a shift in the selectivity of the metal complex, with CO no longer being a major product. One way of rationalizing both the lowering of the overall Faradaic efficiency as well as the decrease in CPE current under CO₂ vs N₂ atmosphere (Figures 3C & 3D, Tables S1 & S2) is through CO inhibition (via irreversible adsorption) of heterogeneous catalytic surface sites. XPS analysis of the post-electrolysis working electrode reveals a cobalt signal following rinsing with acetonitrile, again suggesting the presence of a heterogeneously deposited species (Figure S42). While CO poising is not observed for our previously studied molecular cobalt macrocycles,^{60,61} we cannot rule out such a process occurring with CoL^{NO2}.

Analysis of the post-CPE working solution via UV-vis spectroscopy shows the original absorption of CoL^{NO2} has redshifted from 315 nm to 324 nm (Figure S36). While it is unclear what the exact source of this redshift is, FTIR spectroscopy of the solution in the working compartment of the electrolysis cell (Figure S39) has resolved vibrations attributed to unmodified CoL^{NO2}, which indicates the molecular species remains present in solution, and points to changes in the solution chemical environment. It should be noted that while CoL^{NO2} is detected in the solution phase, this does not rule out partial deposition of CoL^{NO2} onto the electrode surface.

CPE Experiments with H₂O Under a CO₂ Atmosphere

Switching the proton source from TFE to H_2O under a CO_2 atmosphere results in higher currents at -2.70 V vs $Fc^{+/0}$ (Figure 6), which is consistent with the higher currents observed in the CV experiments. H_2 was generated in even higher quantities under these conditions, reaching a maximum faradaic efficiency of 71% after a 6h CPE study, while the FE for CO decreased to \sim 1% (Table S3). After 24 hours, 875 μ mol of H_2 were produced, which is 2.5 times higher than the amount of H_2 produced when TFE was used as the proton source. This increased current and increased H_2 produced is likely due to the presence of H_2CO_3 , generated from the equilibrium reaction of H_2O and CO_2 , which is a significantly stronger acid than TFE (Table S11).

CPE Experiments with Phenol Under a CO₂ Atmosphere

Using 1 M phenol as the proton source resulted in the highest maximum current (Figure 6). However, this current is not stable and begins to rapidly decrease after 2 hours of CPE. The faradaic efficiency for CO under these conditions is similar to that obtained under TFE

conditions, reaching up to 4% (Table S4). Unlike the CPE studies with TFE, or H_2O as the proton sources, the CPE experiment in the presence of PhOH generates the maximum FE for H_2 after 2 hours (46%), which subsequently decreases to 18% at the end of the 24h CPE study. We attribute the decrease in FE% over the course of the experiment to the large amount of H_2 produced, which over-pressurizes the CPE-cell leading to a partial loss of H_2 gas. A replicate experiment using additional securing methods for the CPE-cell displayed no appreciable loss of H_2 between 2 and 8 hours, with an average detected FE for H_2 of 54% (Table S12). After 24 hours some loss of H_2 was observed (FE $_{H2}$ = 42%), and may be attributed to either partial (electro)chemical consumption of H_2 or physical loss due to over-pressurization.

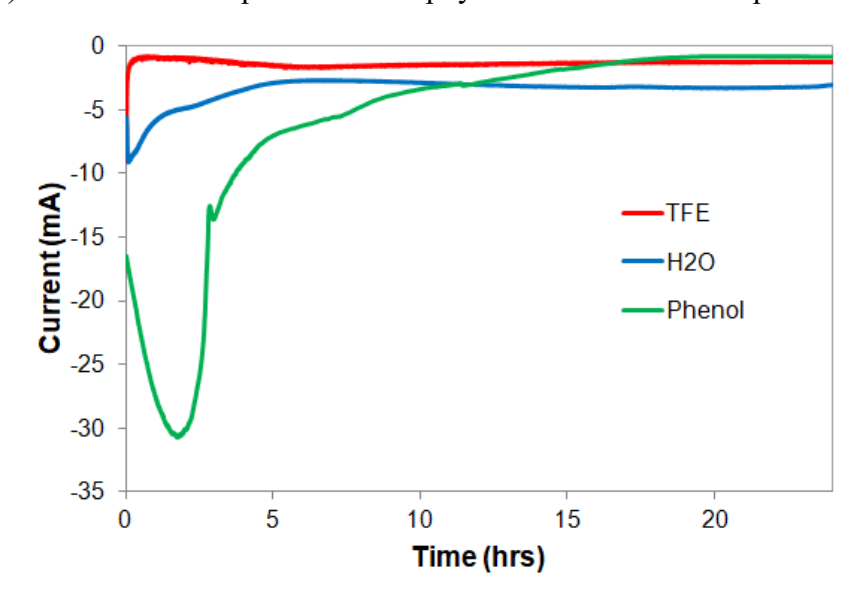


Figure 6. CPE of 0.5 mM **CoL**^{NO2} under CO₂ in 0.1 M TBAPF₆ MeCN solution at –2.70 V vs Fc^{+/0} with 1 M TFE (red), water (blue), and phenol (green) as an added proton source.

The need for polishing between CV scans and the unaccounted for faradaic efficiency raised suspicions of the decomposition of the catalyst, possibly forming cobalt nanoparticles on the electrode surface that may be the active catalyst. A 2 hour controlled potential electrolysis experiment was performed with 1 M phenol (Figure S18), as the high currents generated with phenol followed by a large current drop suggested these conditions might be best suited for promoting catalyst decomposition. Following the electrochemical experiment, the area of the electrode that was in solution was washed with acetonitrile. Half of this washed area of the working electrode was then further washed with dimethylformamide (DMF). Analysis of the

electrode by X-ray photoelectron spectroscopy (XPS) revealed peaks in the Co 2p region for both washed regions (Figure S17), suggesting that a deposited cobalt material is retained on the electrode. Additionally, replicate CPE experiments show variability in the initial three hours of electrolysis (Figure S43), hinting at the possibility of a pre-activation step that is very sensitive to precise catalyst concentration and electrode surface area.

UV-vis and FTIR spectroscopic analyses (Figures S37 and S40) of the post-electrolysis working solution were inconclusive as to whether a molecular species remains in solution, as the absorption and vibrational features were saturated with signals derived from the added phenol. A controlled potential electrolysis experiment performed with the previously washed electrode and 1 M phenol without any added CoL^{NO2} produces about one third of the current seen when 1 M phenol and CoL^{NO2} are used with a clean electrode (Figure S18). The amount of hydrogen produced is also roughly one third of that produced with CoL^{NO2} (Table S5), though the faradaic efficiency is slightly higher for the deposited material at 55%.

We wish to note the lower amount of H₂ produced does not necessarily indicate any heterogeneous materials formed are less effective for HER, but rather the stable deposited species produces less H₂ than the initial solution mixture. The real contributions between homogeneous and heterogeneous species in the initial reaction solution is difficult to quantify due to the possibility of forming meta-stable nanoparticles, which may not be accurately accounted for during rinse tests.^{73,74}

Discussion of CPE Results

The CPE studies of CoL^{NO2} have indicated the addition of the nitrophenyl moiety results in a change in selectivity and electrochemical instability leading to deposition. Attempts at characterizing a reduced nitrophenyl group in the post-electrolysis bulk solution were inconclusive (Figures S35–S40) and more sensitive FTIR spectroelectrochemical experiments are required in the future to better elucidate the structure of the active catalyst. As CoL^{NO2} has all tertiary amines similar to CoL⁶, a loss of CO₂ selectivity is not unexpected; however, the extent of loss was unexpected, going from 36% to 4% FE for CO when comparing CoL⁶ to CoL^{NO2}, as well as the modest to high amount of H₂ formed (Table 2). Several factors may be responsible for this change in behavior from predominately converting CO₂-to-CO, to producing H₂. First, the steric crowding around the metal center could be contributing to this selectivity shift, as

protons require less space than the relatively bulky CO₂. In conjunction with the methyl groups, which have been shown to hinder CO₂ binding, the presence of the nitrophenyl group could further block access to the metal center as well as hinder the formation of important hydrogen bonding intermediates (vide infra). Second, computational studies of the tetra-(NH) complex, CoL¹, have illustrated that the inclusion of pendant NH groups facilities the formation of a hydrogen bonding network with exogenously added acid.⁶¹ These hydrogen bonding interactions are critical for CO₂ binding and the subsequent proton/electron transfer steps required for CO₂to-CO conversion. The absence of NH hydrogen bond donor groups to direct the formation these networks have been shown to reduce the Faradaic efficiency of CO production from 98% for CoL¹ (containing four pendant NH groups) to 36% for CoL⁶ (Table 2). Thirdly, the inclusion of a nitrophenol moiety may lead to the catalyst being overall less electrochemically stable over the course of the experiment as evidenced by the post-electrolysis XPS of the working electrode showing the presence of a heterogeneous cobalt containing material. The deposition process itself, as well as the propensity for the deposited species to perform HER both lower the overall efficiency for CO production. Taken together these factors illustrate the importance of intramolecular hydrogen bonding groups and electrochemically robust functional groups for selective CO₂-to-CO conversion. The absence of these elements in CoL^{NO2} likely both contribute to the homogenous and heterogenous (via deposition) production of H₂.

Cyclic Voltammetry Dependence Studies

Various CV experiments were performed in order to better understand how CoL^{NO2} differs from the unsubstituted cobalt aminopyridine complexes and how to further develop aminopyridine macrocycles with proton donors in different positions to facilitate reduction processes. Due to the irreversible nature of the reduction features of CoL^{NO2} under N_2 , and the peaked nature of the catalytic reactions performed under either N_2 or CO_2 , we were unable to extrapolate true catalytic rate constants. To compare the activity of CoL^{NO2} under protio vs deuterated acid sources, CVs were performed in MeCN solutions of CoL^{NO2} under N_2 in the presence of increasing amounts of H_2O and D_2O (Figures S12, S19, S20), and the values of $(i_{max(H)}/i_{max(D)})^2$ were employed to get mechanistic insights. Under ideal catalytic Nernstian conditions (an S-shaped catalytic wave occurring at a reversible one-electron couple) the

normalized catalytic current $(i_{cat}/i_p)^2$, where i_{cat} = the catalytic current, i_p = the peak current, is proportional to the observed catalytic rate constant.⁷⁵ The electrochemical studies performed here indicate that H₂O results in larger $(i_{max(H)}/i_{max(D)})^2$ values with an average ratio of 13.7 ± 9.2 (Table S6). These results are consistent with the catalytic behavior observed for a hydrogenevolving catalyst.⁷⁶ Specifically, these high $(i_{max(H)}/i_{max(D)})^2$ values (up to 30 at 2.5 M H₂O/D₂O) observed are indicative of a mechanism that involves the formation of a metal-hydride intermediate.

Slightly lower $(i_{\text{max(H)}}/i_{\text{max(D)}})^2$ values are observed when switching the atmosphere from N₂ to CO₂ (Figures S13, S21, S22), with $(i_{\text{max(H)}}/i_{\text{max(D)}})^2$ average ratio values of 3.0 ± 2.0 (Table S7). These results are indicative of a mechanism that is not predominately that of a hydrogenevolving catalyst. The unsubstituted complexes were reported to display less noticeable differences using protio vs deuterated acid sources, which is expected for a mechanism that involves primarily CO₂-to-CO reduction.^{60,61}

Solutions of CoL^{NO2} under various conditions were titrated with TFE, H₂O, and phenol in stepwise increments to observe the shift in the reduction feature at -1.75 V (Figures S23-S25). In all cases, regardless of the identity of the proton source or gaseous atmosphere, an anodic shift was observed. TFE had the greatest rate of increase on the current shift (Figure S23), with phenol being second (Figure S25), and H₂O having the weakest effect (Figure S24). However, phenol produced the largest overall shift in potential (Figure S26). This would be expected for a mechanism that involves the formation of a metal-hydride intermediate, as phenol is the strongest acid under a N2 atmosphere. 77-81 Plotting the potential shift under a N2 atmosphere against the pKa of these acids (Table S11) in acetonitrile produces a line with a slope of 30.2 mV/pH unit (Figure S26), which suggests a two-electron, one-proton event.82 The unsubstituted cobalt aminopyridine complexes showed only two metal-based reduction events that were proton independent, 60,61 so the behavior observed in this study is unique to the nitrophenyl-substituted complex. As mentioned previously, the size of the reduction feature at -1.75 V is noticeably larger than the other two reduction features present in the CVs of CoL^{NO2}. The slope matching a two-electron event further supports that there may be both a ligand reduction and metal reduction at this potential. The metal-based reduction, Co^{II/I}, occurring at this potential would match the Co^{II/I} couple for the unsubstituted cobalt aminopyridine complexes. The proton dependence of the reduction feature at -1.75 V could be indicative of the formation of a Co(III)-hydride intermediate. This would explain the higher selectivity of CoL^{NO2} for HER relative to the unsubstituted cobalt aminopyridine complexes.

The increase in the catalytic current with added protons was also investigated. While the desired S-shaped curve could not be obtained during these studies, analysis of the relationship between proton concentration and current was observed qualitatively. **CoL**^{NO2} under CO₂ and N₂ was titrated with TFE, H₂O, and phenol, and the square of the current densities at –2.70 V vs Fc^{+/0} were plotted against the acid concentration (Figures S27-S32). Under N₂ conditions, a linear dependence on proton concentration was observed, whereas under CO₂ conditions a less clear dependence was identified, due to a more complicated mechanistic pathway. In the case of phenol, only concentrations up to 0.48 M were considered due to changing peak shape at higher concentrations, which may be related to catalyst instability. A linear dependence between the catalytic rate constant and the proton concentration has also been reported for the CO₂ reduction studies by unsubstituted cobalt aminopyridine complexes,^{60,61} which suggests that while product selectivity differs between the unsubstituted complexes and **CoL**^{NO2}, the catalysts do have some shared behavior under certain conditions.

Catalytic activity studies were also performed in the presence of varying amounts of CoL^{NO2}. An electrolyte solution under N₂ with 0.5 M TFE was titrated with CoL^{NO2} up to 0.64 mM. The current initially increased from 0 mM to 0.24 mM before stagnating (Figure S33), suggesting that catalyst saturation occurs at low concentrations. Plotting the square of the current density vs the catalyst concentration, a linear trend is observed for the first three data points (0.08, 0.16, and 0.24 mM), followed by a saturation behavior at higher catalyst concentrations (Figure S34). This saturation behavior indicates the formation of an intermediate, such as a Co(III)-H, which serves as the active catalyst, whereas the initial CoL^{NO2} complex serves as a pre-catalyst. This result, together with the one indicating a shift in the -1.75 V reduction feature in the presence of acids, with a slope of 30.2 mV/pH unit that corresponds to a two-electron, one-proton event, further supports the assignment of the formation of a Co(III)-H intermediate. Our previous reports on the cobalt tetra NH complex (CoL¹) showed a linear dependence between the activity and the concentration of the catalyst, over a much larger concentration range (0.2 mM to 1 mM), with no saturation behavior. Overall, these studies indicate that by modifying the cobalt

aminopyridine species with a nitrophenyl moiety coupled with removing pendant amine hydrogen bond donors, leads to a dramatic change in the reactivity and selectivity of CoL^{NO2} with CO_2 compared to that previously observed for the unsubstituted cobalt aminopyridine complexes.

CONCLUSION

Modifications to a previously reported aminopyridine macrocycle produced a nitrophenyl-modified ligand, LNO2, which was subsequently metallated to generate the corresponding cobalt complex, CoLNO2. The ligand coordinates the metal center in a square planar fashion similar to the previously reported cobalt aminopyridine complexes, where the pendant amines pucker up and down in a saddle-like configuration. In the solid state, the nitro group is positioned over the metal center with a Co–O distance of 2.838(4) Å, suggesting that the pendant nitrophenyl moiety could influence the reactivity of this complex. CV experiments showed current increases under both N₂ and CO₂ with the addition of a proton source, with the N₂ current increases being approximately 30 times higher than those under a CO₂ atmosphere. Controlled potential electrolysis showed high faradaic efficiency for H₂ production under both N₂ and CO₂, with larger quantities of H₂ being produced under a N₂ atmosphere. Small amounts of CO were also detected under an atmosphere of CO₂. X-ray photoelectron spectroscopy reveals the presence of cobalt containing species following rinsing of the post-CPE working electrode. This reactivity is in contrast to that of the previously reported cobalt aminopyridine complexes, which had 98% FE for CO₂ reduction to CO. These findings highlight the importance of the pendant hydrogen bonding amines towards selective CO₂-to-CO conversion where interactions with exogenous acid are likely critical in dictating catalytic selectivity. The addition of a single nitrophenyl moiety while also removing the pendant secondary amines has a large impact on both the catalytic activity and selectivity.

ASSOCIATED CONTENT

Supporting Information

The Supporting Information contains description of experimental methods, synthetic methods, ¹H NMR, FT-IR, UV-Vis, cyclic voltammetry, Randles–Sevcik plots, controlled potential electrolysis, XPS data, and crystal structure tables.

Crystallographic data

ACKNOWLEDGEMENTS

The studies performed here were supported by the National Science Foundation (NSF) through awards CHE-1555387 and CHE-2102707. The authors also acknowledge support from the Alfred P. Sloan Foundation through a Sloan research fellowship to SCM, the University of Southern California (USC) Wrigley Institute for the Norma and Jerol Sonosky summer fellowship to EMJ and for the Phil and Susan Hagenah postdoctoral fellowship to JJL, and to Thomas Moulton and Ginny Dunn for the Harold and Lillian Moulton Graduate Fellowship to EMJ. The authors are grateful to NSF (grant CRIF 1048807) and USC for their sponsorship of NMR spectrometers and X-ray diffractometer. The authors also thank Dr. Alon Chapovetsky for discussion.

REFERENCES

- (1) Lewis, N. S.; Nocera, D. G. Powering the Planet: Chemical Challenges in Solar Energy Utilization. *Proc. Natl. Acad. Sci.* **2006**, *103*, 15729–15735.
- (2) Chu, S.; Majumdar, A. Opportunities and Challenges for a Sustainable Energy Future. *Nature* **2012**, *488*, 294–303.
- (3) Seh, Z. W.; Kibsgaard, J.; Dickens, C. F.; Chorkendorff, I.; Nørskov, J. K.; Jaramillo, T. F. Combining Theory and Experiment in Electrocatalysis: Insights into Materials Design. *Science* **2017**, *355*, eaad4998.
- (4) De Luna, P.; Hahn, C.; Higgins, D.; Jaffer, S. A.; Jaramillo, T. F.; Sargent, E. H. What Would It Take for Renewably Powered Electrosynthesis to Displace Petrochemical Processes? *Science* **2019**, *364*.
- (5) Francke, R.; Schille, B.; Roemelt, M. Homogeneously Catalyzed Electroreduction of Carbon Dioxide Methods, Mechanisms, and Catalysts. *Chem. Rev.* **2018**, *118*, 4631–4701.
- (6) Tatin, A.; Bonin, J.; Robert, M. A Case for Electrofuels. *ACS Energy Lett.* **2016**, *1*, 1062–1064.
- (7) Cen, J.; Wu, Q.; Liu, M.; Orlov, A. Developing New Understanding of Photoelectrochemical Water Splitting via In-Situ Techniques: A Review on Recent Progress. *Green Energy Environ.* **2017**, *2*, 100–111.

- (8) Appel, A. M.; Bercaw, J. E.; Bocarsly, A. B.; Dobbek, H.; DuBois, D. L.; Dupuis, M.; Ferry, J. G.; Fujita, E.; Hille, R.; Kenis, P. J. A.; et al. Frontiers, Opportunities, and Challenges in Biochemical and Chemical Catalysis of CO₂ Fixation. *Chem. Rev.* **2013**, *113*, 6621–6658.
- (9) Whipple, D. T.; Kenis, P. J. A. Prospects of CO₂ Utilization via Direct Heterogeneous Electrochemical Reduction. *J. Phys. Chem. Lett.* **2010**, *1*, 3451–3458.
- (10) Jiao, Y.; Zheng, Y.; Jaroniec, M.; Qiao, S. Z. Design of Electrocatalysts for Oxygen- and Hydrogen-Involving Energy Conversion Reactions. *Chem. Soc. Rev.* **2015**, *44*, 2060–2086.
- (11) Benck, J. D.; Hellstern, T. R.; Kibsgaard, J.; Chakthranont, P.; Jaramillo, T. F. Catalyzing the Hydrogen Evolution Reaction (HER) with Molybdenum Sulfide Nanomaterials. *ACS Catal.* **2014**, *4*, 3957–3971.
- (12) Pegis, M. L.; Wise, C. F.; Martin, D. J.; Mayer, J. M. Oxygen Reduction by Homogeneous Molecular Catalysts and Electrocatalysts. *Chem. Rev.* **2018**, *118*, 2340–2391.
- (13) Gasteiger, H. A.; Kocha, S. S.; Sompalli, B.; Wagner, F. T. Activity Benchmarks and Requirements for Pt, Pt-Alloy, and Non-Pt Oxygen Reduction Catalysts for PEMFCs. *Appl. Catal. B Environ.* **2005**, *56*, 9–35.
- (14) Gasteiger, H. A.; Marković, N. M. Just a Dream—or Future Reality? *Science* **2009**, *324*, 48–49.
- (15) Rosen, B. A.; Salehi-khojin, A.; Thorson, M. R.; Zhu, W.; Whipple, D. T.; Kenis, P. J. A.; Masel, R. I. Ionic Liquid Mediated Selective Conversion of CO₂ to CO At Low Overpotentials. *Science* **2011**, *334*, 643–644.
- (16) Qiao, J.; Liu, Y.; Hong, F.; Zhang, J. A Review of Catalysts for the Electroreduction of Carbon Dioxide to Produce Low-Carbon Fuels; 2014; Vol. 43.
- (17) Boutin, E.; Merakeb, L.; Ma, B.; Boudy, B.; Wang, M.; Bonin, J.; Anxolabéhère-Mallart, E.; Robert, M. Molecular Catalysis of CO₂ reduction: Recent Advances and Perspectives in Electrochemical and Light-Driven Processes with Selected Fe, Ni and Co Aza Macrocyclic and Polypyridine Complexes. *Chem. Soc. Rev.* **2020**, *49*, 5772–5809.
- (18) Azcarate, I.; Costentin, C.; Robert, M.; Savéant, J. M. Dissection of Electronic Substituent Effects in Multielectron-Multistep Molecular Catalysis. Electrochemical CO₂-to-CO Conversion Catalyzed by Iron Porphyrins. *J. Phys. Chem. C* **2016**, *120*, 28951–28960.
- (19) Azcarate, I.; Costentin, C.; Robert, M.; Savéant, J. M. Through-Space Charge Interaction Substituent Effects in Molecular Catalysis Leading to the Design of the Most Efficient Catalyst of CO₂-to-CO Electrochemical Conversion. *J. Am. Chem. Soc.* **2016**, *138*, 16639–16644.
- (20) Costentin, C.; Drouet, S.; Robert, M.; Savéant, J.-M. A Local Proton Source Enhances CO₂ Electroreduction to CO by a Molecular Fe Catalyst. *Science* **2012**, *338*, 90–94.
- (21) Costentin, C.; Robert, M.; Savéant, J. M. Catalysis of the Electrochemical Reduction of Carbon Dioxide. *Chem. Soc. Rev.* **2013**, *42*, 2423–2436.
- (22) Costentin, C.; Drouet, S.; Passard, G.; Robert, M.; Savéant, J. M. Proton-Coupled Electron Transfer Cleavage of Heavy-Atom Bonds in Electrocatalytic Processes. Cleavage of a C-O Bond in the Catalyzed Electrochemical Reduction of CO₂. J. Am. Chem. Soc. 2013, 135, 9023–9031.
- (23) Costentin, C.; Passard, G.; Robert, M.; Savéant, J.-M. Pendant Acid–Base Groups in Molecular Catalysts: H-Bond Promoters or Proton Relays? Mechanisms of the Conversion

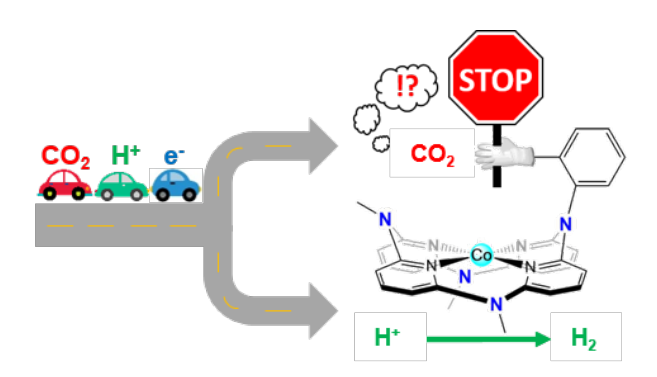
- of CO₂ to CO by Electrogenerated Iron(0)Porphyrins Bearing Prepositioned Phenol Functionalities. *J. Am. Chem. Soc.* **2014**, *136*, 11821–11829.
- (24) Costentin, C.; Robert, M.; Savéant, J.-M.; Tatin, A. Efficient and Selective Molecular Catalyst for the CO₂-to-CO Electrochemical Conversion in Water. *Proc. Natl. Acad. Sci.* **2015**, *112*, 6882–6886.
- (25) Bhugun, I.; Lexa, D.; Savéant, J. M. Catalysis of the Electrochemical Reduction of Carbon Dioxide by Iron(0) Porphyrins. Synergistic Effect of Lewis Acid Cations. *J. Phys. Chem.* **1996**, *100*, 19981–19985.
- (26) Hammouche, M.; Lexa, D.; Savêant, J. M.; Momenteau, M. Chemical Catalysis of Electrochemical Reactions. Homogeneous Catalysis of the Electrochemical Reduction of Carbon Dioxide by Iron("0") Porphyrins. Role of the Addition of Magnesium Cations. *J. Am. Chem. Soc.* **1991**, *113*, 8455–8466.
- (27) Bhugun, I.; Lexa, D.; Savéant, J. M. Catalysis of the Electrochemical Reduction of Carbon Dioxide by Iron(0) Porphyrins: Synergystic Effect of Weak Brönsted Acids. *J. Am. Chem. Soc.* **1996**, *118*, 1769–1776.
- (28) Bhugun, I.; Lexa, D.; Savéant, J. M. Ultraefficient Selective Homogeneous Catalysis of the Electrochemical Reduction of Carbon Dioxide by an Iron(0) Porphyrin Associated with a Weak Brönsted Acid Cocatalyst. *J. Am. Chem. Soc.* **1994**, *116*, 5015–5016.
- (29) Abe, T.; Taguchi, F.; Imaya, H.; Zhao, F.; Zhang, J.; Kaneko, M. Highly Active Electrocatalysis by Cobalt Tetraphenylporphyrin Incorporated in a Nafion Membrane for Proton Reduction. *Polym. Adv. Technol.* **1998**, *9*, 559–562.
- (30) Kleingardner, J. G.; Kandemir, B.; Bren, K. L. Hydrogen Evolution from Neutral Water under Aerobic Conditions Catalyzed by Cobalt Microperoxidase-11. *J. Am. Chem. Soc.* **2014**, *136*, 4–7.
- (31) Kellett, R. M.; Spiro, T. G. Cobalt Porphyrin Electrode Films as H₂ Evolution Catalysts. *Inorg. Chem.* **1985**, *24*, 2378–2382.
- (32) Kellett, R. M.; Spiro, T. G. Cobalt(I) Porphyrin Catalysis of Hydrogen Production from Water. *Inorg. Chem.* **1985**, *24*, 2373–2377.
- (33) Beyene, B. B.; Mane, S. B.; Hung, C. H. Highly Efficient Electrocatalytic Hydrogen Evolution from Neutral Aqueous Solution by a Water-Soluble Anionic Cobalt(II) Porphyrin. *Chem. Commun.* **2015**, *51*, 15067–15070.
- (34) Beyene, B. B.; Mane, S. B.; Hung, C.-H. Electrochemical Hydrogen Evolution by Cobalt (II) Porphyrins: Effects of Ligand Modification on Catalytic Activity, Efficiency and Overpotential. *J. Electrochem. Soc.* **2018**, *165*, H481–H487.
- (35) Dogutan, D. K.; Bediako, D. K.; Graham, D. J.; Lemon, C. M.; Nocera, D. G. Proton-Coupled Electron Transfer Chemistry of Hangman Macrocycles: Hydrogen and Oxygen Evolution Reactions. *J. Porphyr. Phthalocyanines* **2015**, *19*, 1–8.
- (36) Kielb, P.; Horch, M.; Wrzolek, P.; Goetz, R.; Ly, K. H.; Kozuch, J.; Schwalbe, M.; Weidinger, I. M. Hydrogen Evolution by Cobalt Hangman Porphyrins under Operating Conditions Studied by Vibrational Spectro-Electrochemistry. *Catal. Sci. Technol.* **2018**, *8*, 1849–1857.
- (37) Lee, C. H.; Dogutan, D. K.; Nocera, D. G. Hydrogen Generation by Hangman Metalloporphyrins. *J. Am. Chem. Soc.* **2011**, *133*, 8775–8777.
- (38) Roubelakis, M. M.; Bediako, D. K.; Dogutan, D. K.; Nocera, D. G. Proton-Coupled Electron Transfer Kinetics for the Hydrogen Evolution Reaction of Hangman Porphyrins.

- Energy Environ. Sci. 2012, 5, 7737–7740.
- (39) Huang, D.; Lu, J.; Li, S.; Luo, Y.; Zhao, C.; Hu, B.; Wang, M.; Shen, Y. Fabrication of Cobalt Porphyrin. Electrochemically Reduced Graphene Oxide Hybrid Films for Electrocatalytic Hydrogen Evolution in Aqueous Solution. *Langmuir* **2014**, *30*, 6990–6998.
- (40) Beley, M.; Collin, J.-P.; Ruppert, R.; Sauvage, J.-P. Nickel(II)-Cyclam: An Extremely Selective Electrocatalyst for Reduction of CO₂ in Water. *J. Chem. Soc. Chem. Commun.* **1984**, *2*, 1315.
- (41) Beley, M.; Collin, J. P.; Ruppert, R.; Sauvage, J. P. Electrocatalytic Reduction of Carbon Dioxide by Nickel Cyclam²⁺ in Water: Study of the Factors Affecting the Efficiency and the Selectivity of the Process. *J. Am. Chem. Soc.* **1986**, *108*, 7461–7467.
- (42) Collin, J. P.; Jouaiti, A.; Sauvage, J. P. Electrocatalytic Properties of Nickel(Cyclam)²⁺ and Ni₂(Biscyclam)⁴⁺ with Respect to CO₂ and H₂O Reduction. *Inorg. Chem.* **1988**, *27*, 1986–1990.
- (43) Froehlich, J. D.; Kubiak, C. P. Homogeneous CO₂ Reduction by Ni(Cyclam) at a Glassy Carbon Electrode. *Inorg. Chem.* **2012**, *51*, 3932–3934.
- (44) Froehlich, J. D.; Kubiak, C. P. The Homogeneous Reduction of CO₂ by [Ni(Cyclam)]⁺: Increased Catalytic Rates with the Addition of a CO Scavenger. *J. Am. Chem. Soc.* **2015**, *137*, 3565–3573.
- (45) Schneider, J.; Jia, H.; Kobiro, K.; Cabelli, D. E.; Muckerman, J. T.; Fujita, E. Nickel(II) Macrocycles: Highly Efficient Electrocatalysts for the Selective Reduction of CO₂ to CO. *Energy Environ. Sci.* **2012**, *5*, 9502.
- (46) Song, J.; Klein, E. L.; Neese, F.; Ye, S. The Mechanism of Homogeneous CO₂ Reduction by Ni(Cyclam): Product Selectivity, Concerted Proton–Electron Transfer and C–O Bond Cleavage. *Inorg. Chem.* **2014**, *53*, 7500–7507.
- (47) Neri, G.; Aldous, I. M.; Walsh, J. J.; Hardwick, L. J.; Cowan, A. J. A Highly Active Nickel Electrocatalyst Shows Excellent Selectivity for CO₂ Reduction in Acidic Media. *Chem. Sci.* **2016**, *7*, 1521–1526.
- (48) Amanullah, S.; Saha, P.; Nayek, A.; Ahmed, M. E.; Dey, A. Biochemical and Artificial Pathways for the Reduction of Carbon Dioxide, Nitrite and the Competing Proton Reduction: Effect of 2nd sphere Interactions in Catalysis. *Chem. Soc. Rev.* **2021**, *50*, 3755–3823.
- (49) Ahmed, M. E.; Rana, A.; Saha, R.; Dey, S.; Dey, A. Homogeneous Electrochemical Reduction of CO₂ to CO by a Cobalt Pyridine Thiolate Complex. *Inorg. Chem.* **2020**, *59*, 5292–5302.
- (50) Dey, S.; Todorova, T. K.; Fontecave, M.; Mougel, V. Electroreduction of CO₂ to Formate with Low Overpotential Using Cobalt Pyridine Thiolate Complexes. *Angew. Chem. Int. Ed.* **2020**, *59*, 15726–15733.
- (51) Dey, S.; Ahmed, M. E.; Dey, A. Activation of Co(I) State in a Cobalt-Dithiolato Catalyst for Selective and Efficient CO₂ Reduction to CO. *Inorg. Chem.* **2018**, *57*, 5939–5947.
- (52) Chen, L.; Guo, Z.; Wei, X. G.; Gallenkamp, C.; Bonin, J.; Anxolabéhère-Mallart, E.; Lau, K. C.; Lau, T. C.; Robert, M. Molecular Catalysis of the Electrochemical and Photochemical Reduction of CO₂ with Earth-Abundant Metal Complexes. Selective Production of CO vs HCOOH by Switching of the Metal Center. *J. Am. Chem. Soc.* 2015, 137, 10918–10921.

- (53) Rail, M. D.; Berben, L. A. Directing the Reactivity of [HFe₄N(CO)₁₂]. *J. Am. Chem. Soc.* **2011**, *133*, 18577–18579.
- (54) Taheri, A.; Thompson, E. J.; Fettinger, J. C.; Berben, L. A. An Iron Electrocatalyst for Selective Reduction of CO₂ to Formate in Water: Including Thermochemical Insights. *ACS Catal.* **2015**, *5*, 7140–7151.
- (55) Taheri, A.; Berben, L. A. Making C-H Bonds with CO₂: Production of Formate by Molecular Electrocatalysts. *Chem. Commun.* **2016**, *52*, 1768–1777.
- (56) Loewen, N. D.; Thompson, E. J.; Kagan, M.; Banales, C. L.; Myers, T. W.; Fettinger, J. C.; Berben, L. A. A Pendant Proton Shuttle on [Fe₄N(CO)₁₂]⁻ Alters Product Selectivity in Formate vs. H₂ Production via the Hydride [H-Fe₄N(CO)₁₂]⁻. *Chem. Sci.* **2016**, *7*, 2728–2735.
- (57) Loewen, N. D.; Berben, L. A. Secondary Coordination Sphere Design to Modify Transport of Protons and CO₂. *Inorg. Chem.* **2019**, *58*, 16849–16857.
- (58) Franco, F.; Cometto, C.; Nencini, L.; Barolo, C.; Sordello, F.; Minero, C.; Fiedler, J.; Robert, M.; Gobetto, R.; Nervi, C. Local Proton Source in Electrocatalytic CO₂ Reduction with [Mn(Bpy–R)(CO)₃Br] Complexes. *Chem. Eur. J.* **2017**, *23*, 4782–4793.
- (59) Hellman, A. N.; Haiges, R.; Marinescu, S. C. Influence of Intermolecular Hydrogen Bonding Interactions on the Electrocatalytic Reduction of CO₂ to CO by 6,6'-Amine Substituted Rhenium Bipyridine Complexes. *ChemElectroChem* **2021**, *8*, 1864–1872.
- (60) Chapovetsky, A.; Do, T. H.; Haiges, R.; Takase, M. K.; Marinescu, S. C. Proton-Assisted Reduction of CO₂ by Cobalt Aminopyridine Macrocycles. *J. Am. Chem. Soc.* **2016**, *138*, 5765–5768.
- (61) Chapovetsky, A.; Welborn, M.; Luna, J. M.; Haiges, R.; Miller, T. F.; Marinescu, S. C. Pendant Hydrogen-Bond Donors in Cobalt Catalysts Independently Enhance CO₂ Reduction. ACS Cent. Sci. 2018, 4, 397–404.
- (62) Nichols, E. M.; Derrick, J. S.; Nistanaki, S. K.; Smith, P. T.; Chang, C. J. Positional Effects of Second-Sphere Amide Pendants on Electrochemical CO₂ Reduction Catalyzed by Iron Porphyrins. *Chem. Sci.* **2018**, *9*, 2952–2960.
- (63) Zhang, E.-X.; Wang, D.-X.; Huang, Z.-T.; Wang, M.-X. Synthesis of (NH)_m (NMe)_{4-m}-Bridged Calix[4]Pyridines and the Effect of NH Bridge on Structure and Properties. *J. Org. Chem.* **2009**, *74*, 8595–8603.
- (64) Fang, Y. X.; Ao, Y. F.; Wang, D. X.; Zhao, L.; Wang, M. X. Synthesis, Structure and Transition Metal Ion Complexation Property of Lariat Azacalix[4]Pyridines. *Tetrahedron* **2015**, *71*, 2105–2112.
- (65) Mantina, M.; Chamberlin, A. C.; Valero, R.; Cramer, C. J.; Truhlar, D. G. Consistent van Der Waals Radü for the Whole Main Group. *J. Phys. Chem. A* **2009**, *113*, 5806–5812.
- (66) Batsanov, S. S. Van Der Waals Radii of Elements. *Inorg. Mater.* **2001**, *37*, 871–885.
- (67) Su, X.; McCardle, K. M.; Chen, L.; Panetier, J. A.; Jurss, J. W. Robust and Selective Cobalt Catalysts Bearing Redox-Active Bipyridyl-*N*-Heterocyclic Carbene Frameworks for Electrochemical CO₂ Reduction in Aqueous Solutions. *ACS Catal.* **2019**, *9*, 7398–7408.
- (68) Kleperis, J.; Wójcik, G.; Czerwinski, A.; Skowronski, J.; Kopczyk, M.; Beltowska-Brzezinska, M. Electrochemical Behavior of Metal Hydrides. *J. Solid State Electrochem.* **2001**, *5*, 229–249.
- (69) Gangi, D. A.; Durand, R. R. Binding of Carbon Dioxide to Cobalt and Nickel Tetra-Aza

- Macrocycles. J. Chem. Soc. Chem. Commun. 1986, No. 9, 697-699.
- (70) Schmidt, M. H.; Miskelly, G. M.; Lewis, N. S. Effects of Redox Potential, Steric Configuration, Solvent, and Alkali Metal Cations on the Binding of Carbon Dioxide to Cobalt(I) and Nickel(I) Macrocycles. *J. Am. Chem. Soc.* **1990**, *112*, 3420–3426.
- (71) Sun, Y.; Bigi, J. P.; Piro, N. A.; Tang, M. L.; Long, J. R.; Chang, C. J. Molecular Cobalt Pentapyridine Catalysts for Generating Hydrogen from Water. *J. Am. Chem. Soc.* **2011**, *133*, 9212–9215.
- (72) Margarit, C. G.; Asimow, N. G.; Costentin, C.; Nocera, D. G. Tertiary Amine-Assisted Electroreduction of Carbon Dioxide to Formate Catalyzed by Iron Tetraphenylporphyrin. *ACS Energy Lett.* **2020**, *5*, 72–78.
- (73) Kaeffer, N.; Morozan, A.; Fize, J.; Martinez, E.; Guetaz, L.; Artero, V. The Dark Side of Molecular Catalysis: Diimine–Dioxime Cobalt Complexes Are Not the Actual Hydrogen Evolution Electrocatalyst in Acidic Aqueous Solutions. ACS Catal. 2016, 6, 3727–3737.
- (74) Lee, K. J.; McCarthy, B. D.; Dempsey, J. L. On Decomposition, Degradation, and Voltammetric Deviation: The Electrochemist's Field Guide to Identifying Precatalyst Transformation. *Chem. Soc. Rev.* **2019**, *48*, 2927–2945.
- (75) Costentin, C.; Savéant, J.-M. Multielectron, Multistep Molecular Catalysis of Electrochemical Reactions: Benchmarking of Homogeneous Catalysts. *ChemElectroChem* **2014**, *1*, 1226–1236.
- (76) Nichols, A. W.; Chatterjee, S.; Sabat, M.; MacHan, C. W. Electrocatalytic Reduction of CO₂ to Formate by an Iron Schiff Base Complex. *Inorg. Chem.* **2018**, *57*, 2111–2121.
- (77) Riplinger, C.; Carter, E. A. Influence of Weak Bronsted Acids on Electrocatalytic CO₂ Reduction by Manganese and Rhenium Bipyridine Catalysts. *ACS Catal.* **2015**, *5*, 900–908.
- (78) Clark, M. L.; Cheung, P. L.; Lessio, M.; Carter, E. A.; Kubiak, C. P. Kinetic and Mechanistic Effects of Bipyridine (Bpy) Substituent, Labile Ligand, and Brønsted Acid on Electrocatalytic CO₂ Reduction by Re(Bpy) Complexes. *ACS Catal.* **2018**, *8*, 2021–2029.
- (79) McCarthy, B. D.; Martin, D. J.; Rountree, E. S.; Ullman, A. C.; Dempsey, J. L. Electrochemical Reduction of Brønsted Acids by Glassy Carbon in Acetonitrile-Implications for Electrocatalytic Hydrogen Evolution. *Inorg. Chem.* **2014**, *53*, 8350–8361.
- (80) Ngo, K. T.; McKinnon, M.; Mahanti, B.; Narayanan, R.; Grills, D. C.; Ertem, M. Z.; Rochford, J. Turning on the Protonation-First Pathway for Electrocatalytic CO₂ Reduction by Manganese Bipyridyl Tricarbonyl Complexes. *J. Am. Chem. Soc.* **2017**, *139*, 2604–2618.
- (81) Lam, Y. C.; Nielsen, R. J.; Gray, H. B.; Goddard, W. A. A Mn Bipyrimidine Catalyst Predicted to Reduce CO₂ at Lower Overpotential. *ACS Catal.* **2015**, *5*, 2521–2528.
- (82) McCarthy, B. D.; Dempsey, J. L. Decoding Proton-Coupled Electron Transfer with Potential–p*K*_a Diagrams. *Inorg. Chem.* **2017**, *56*, 1225–1231.

TOC



Synopsis

A cobalt aminopyridine complex was modified with a nitrophenyl group to explore the electronic and steric effects of this group on catalysis. Cyclic voltammetry experiments show current enhancements with added acids under both CO₂ and N₂, with the increase under N₂ being roughly 30 times greater. Product analysis following electrolysis experiments show that the introduction of the nitrophenyl moiety shifts the catalyst selectivity from CO₂ reduction to H₂ evolution, while also incurring heterogeneous surface deposition.